T2R2 東京工業大学リサーチリポジトリ
Tokyo Tech Research Repository

論文 / 著書情報
Article / Book Information

Title	Development of Ultra-Thin CoPt Films With Electrodeposition for 3-D Domain Wall Motion Memory
Authors	T. Huang, Y. Takamura, M. Saito, Md. M. Hasan, S. Kasai, Y. Sonobe, S. Nakagawa
Citation	IEEE Transactions on Magnetics, Vol. 59, Issue 11, pp. 1-5
Pub. date	2023, 7
Copyright	(c) 2023 IEEE. Personal use of this material is permitted. Permission from IEEE must be obtained for all other uses, in any current or future media, including reprinting/republishing this material for advertising or promotional purposes, creating new collective works, for resale or redistribution to servers or lists, or reuse of any copyrighted component of this work in other works.
DOI	http://dx.doi.org/10.1109/TMAG.2023.3298911
Note	This file is author (final) version.

Powered by T2R2 (Tokyo Institute Research Repository)

This article has been accepted for publication in IEEE Transactions on Magnetics. This is the author's version which has not been fully edited and content may change prior to final publication. Citation information: DOI 10.1109/TMAG.2023.3298911

Development of Ultra-thin CoPt Films with Electrodeposition for Three-dimensional Domain Wall Motion Memory

Tongshuang Huang[1], Yota Takamura[1], *IEEE, Member*, Mikiko Saito[2], Md. Mahmudul Hasan[2], Shinya Kasai[3], Yoshiaki Sonobe[2] *IEEE, Senior Member*, and Shigeki Nakagawa[1] *IEEE, Member*

[1]Dept. of Electrical and Electronic Eng., Tokyo Institute of Technology 2-12-1 Ookayama, Meguro-ku, Tokyo, 152-8552, Japan
[2]Research Organization for Nano and Life Innovation, Waseda University, Shinjuku, Tokyo, 162-0041, Japan
[3]Research Center for Magnetic and Spintronic Materials, NIMS 1-2-1 Sengen, Tsukuba-shi, Ibaraki, 305-0047, Japan

The authors developed the electrodeposition technique for CoPt thin films applicable to three-dimensional domain motion memory (3D-DWMM). CoPt films with perpendicular magnetic anisotropy (PMA) were obtained in a wide range of the Co composition which was controlled by adjusting the potential during electrodeposition. The magnetic properties of the CoPt films were controlled via the Co composition. The pulse electrodeposition method was conducted to obtain smooth morphology of the $Co_{68}Pt_{32}$ films. Ultra-thin $Co_{68}Pt_{32}$ films with smooth surface morphology and an excellent squareness ratio were obtained. This study promises the electrodeposition of the artificial ferromagnetic multilayers for the magnetic pillar of the 3D-DWMM can be achieved.

***Index Terms*—Cobalt-Platinum alloy, electrodeposition, perpendicular magnetic anisotropy (PMA), spin-orbit-torque (SOT)**

I. Introduction

Recently, a three-dimensional domain wall motion memory (3D-DWMM) has been proposed as an information storage device that suits the requirements of both high storage density and fast read/write speed simultaneously [1,2]. The 3D-DWMM consists of magnetic pillars placed vertically on the bit lines. Each magnetic pillar stores multiple bits as it is composed of many magnetic layers, contributing to the high storage density. To achieve high density structure, the diameter of the magnetic pillars should be in the hundreds of nanometers range while the height should be in the micrometer range since the dimension directly affect the bit density.

In 3D-DWMM, each magnetic pillar has a periodically multilayered structure consisting of two magnetic layers: the strong coupling layer (SCL) and the weak coupling layer (WCL) [1,2]. The SCLs have large magnetic anisotropy (K_u) along with perpendicular magnetic anisotropy (PMA) and large exchange stiffness (A_{ex}) and thus hold magnetization to store the data. On the other hand, the WCLs have lower K_u and serve as domain wall pinned layers to separate the magnetization of SCLs.

Current-induced spin-orbit torque (SOT) magnetization switching (MS) is a promising writing method for 3D-DWMM [3-5]. Therefore, the bit line is made of heavy metals (HMs) with considerable spin-orbit interaction. A smooth interface between the HM and the bottom ferromagnetic layer of the magnetic pillars is required. Note that the bottom layer is the SCL.

CoPt alloy is an attractive material for the magnetic pillars of 3D-DWMM because they can have PMA owing to magnetocrystalline anisotropy of the hexagonal close packed (hcp) structure, depending on the Co composition. In addition, their magnetic properties can be tuned by the composition [6,7]. Strong PMA, a desirable property for SCLs, can be obtained in Co-rich CoPt alloy in the hcp phase [8,9], while WCLs can be achieved in Pt-rich CoPt alloys. The magnetic multilayers with magnetic properties modulated periodically can be achieved by a stack of CoPt multilayers with two different Co compositions. This stack needs to be formed sequentially without exposure to air to achieve effective domain motion. Very recently, a study in CoPt multilayered nanowires by electrodeposition was conducted, which supports the feasibility of the fabrication of magnetic pillars [10].

The feasible fabrication process of the magnetic pillars is to fill the micrometer deep, nanometers diameters, holes in insulators such as SiO_2 with magnetic materials. The electrodeposition method is promising for forming magnetic pillars since ions can be brought through nanometer-scale holes to the interface between the electrodes and the solution, forming alloys on the electrode. The electrodeposition technique can control the composition of CoPt alloys by adjusting the applied potential. Note that a sputtering method, commonly employed to form magnetic memories based on spintronics, is unsuitable for this application since it could make clogs near the opening of the micrometer-deep holes.

In this paper, we successfully controlled the magnetic properties of electrodeposited CoPt single layers with different compositions by adjusting the applied potential. In addition,

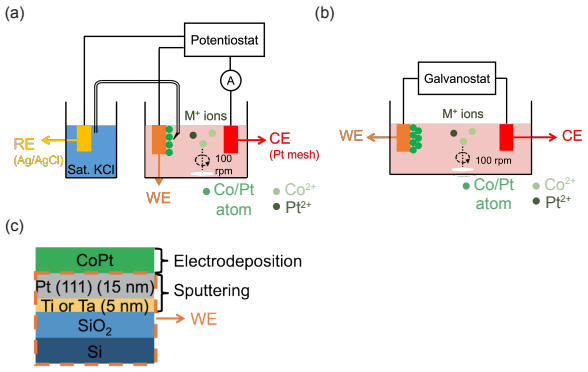

Fig. 1. Experimental setup for (a) DC electrodeposition and (b) pulse electrodeposition. (c) Sample structure.

Manuscript received April 1, 2015; revised May 15, 2015 and June 1, 2015; accepted July 1, 2015. Date of publication July 10, 2015; date of current version July 31, 2015.
Corresponding author: Y. Takamura (email: takamura@ee.e.titech.ac.jp),
Digital Object Identifier (inserted by IEEE).

0018-9464 © 2015 IEEE. Personal use is permitted, but republication/redistribution requires IEEE permission.
See http://www.ieee.org/publications_standards/publications/rights/index.html for more information. (Inserted by IEEE.)
© 2023 IEEE. Personal use is permitted, but republication/redistribution requires IEEE permission. See https://www.ieee.org/publications/rights/index.html for more information.

This article has been accepted for publication in IEEE Transactions on Magnetics. This is the author's version which has not been fully edited and content may change prior to final publication. Citation information: DOI 10.1109/TMAG.2023.3298911

ultra-thin $Co_{68}Pt_{32}$ films with a smooth surface and strong PMA were achieved by pulse electrodeposition.

II. Experimental

A. Electrodeposition conditions

Figs. 1(a) and (b) show experimental configurations of our DC and pulse electrodeposition systems, respectively. The three electrodes system was used in the DC electrodeposition to control a potential between the working electrode (WE) and the reference electrode (RE) [11]. On the other hand, the two electrodes system was used in pulse electrodeposition. The WE was a Pt (15 nm)/ non-magnetic (NM) metal (5 nm)/SiO_2/Si, as shown in Fig. 1(c), where the number in parentheses is the thickness of each layer. The NM material was Ti or Ta. Both Pt and NM layers were deposited using a sputtering method. The Pt layer had a highly (111) oriented structure with the face-centered cubic (fcc) structure.

The electrodeposition conditions used for both DC and pulse methods are shown in Table I. Pt mesh and Ag/AgCl (sat. KCl) were used as counter electrode (CE) and reference electrode (RE), respectively. The solution temperature was maintained at 30°C using a constant temperature bath. The agitation speed was 100 rpm. The pH of the solution was adjusted to 5.2 by adding 0.1 M of NaOH solution. Referring to previous reports [7,12], 0.001 M of diammine dinitro Platinum (II) [$Pt(NO_2)_2(NH_3)_2$] and 0.1 M of Cobalt (II) sulfate heptahydrate [$CoSO_4.7H_2O$ (0.1 M)] were used. We also used diammonium citrate [$(NH_4)_2C_6H_6O_7$] and glycine [NH_2CH_2COOH] to obtain uniform grains in a dense and even morphology with fewer defects in CoPt thin films [13,14]. The diammine dinitro Platinum (II) was produced by Kojima Chemicals Co., Ltd. The other chemicals were produced by Kanto Chemical Co., Inc.

B. Characterization methods

The film thickness was measured using a profilometer (P-15, KLA-Tencore Corporation). The composition of CoPt layers was characterized by glow discharge optical emission spectrometry (rf-GD-OES, Horiba, Ltd.). The magnetic property was measured with a vibrating-sample magnetometer (VSM BHV-3,5 series, Riken Denshi Co., Ltd.). The crystal structure of the samples was determined using an x-ray diffractometer (RINT-2000, XRD, Rigaku Corporation). The surface morphology was characterized by atomic force microscopy (AFM 100 series, AFM, Hitachi High-Tech Co., Ltd.). Regarding the microstructure of CoPt films, after being processed by a focused ion beam, cross-section views of the samples were observed by transmission electron microscopy (JEM-2010F, TEM, JEOL Co., Ltd.).

TABLE I
Electrodeposition Conditions

Counter electrode (CE)	Pt mesh
Reference electrode (RE)	Ag/AgCl (sat. KCl)
Bath temperature	30 °C
Agitation	100 rpm
pH	5.2
Bath composition	$Pt(NO_2)_2(NH_3)_2$ (0.001 M)
	$CoSO_4 \cdot 7H_2O$ (0.1 M)
	$(NH_4)_2C_6H_6O_7$ (0.1 M)
	NH_2CH_2COOH (0.1 M)

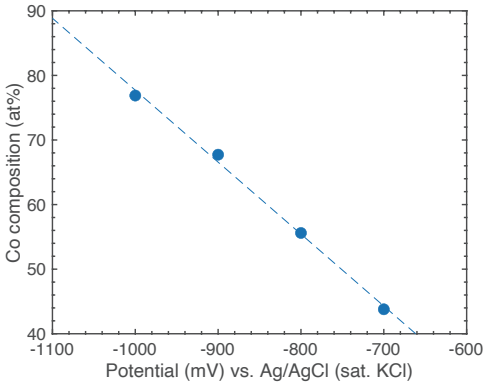

Fig. 2. Co composition of CoPt films as a function of the applied potential.

III. Results

A. Control of the magnetic properties of CoPt alloy with DC electrodeposition

First, we carried out electrochemical deposition using a DC power supply. The potential between WE and RE varied from −700 mV to −1000 mV. The thickness of the CoPt layers was fixed in a range of 24 ± 3 nm unless otherwise noted.

Fig. 2 shows the Co composition of fabricated CoPt layers as a function of the potential between WE and RE. The Co composition showed a linear relationship with the applied potential, ranging from 44% to 77% within the potential range of −700 mV to −1000 mV. Potentials lower than −700 mV resulted in an extremely slow deposition rate. Meanwhile, potentials higher than -1000 mV triggered strong hydrogen gas generation, which can deteriorate the morphology. These results demonstrate the feasibility of depositing both Pt-rich and Co-rich CoPt alloy using a single solution.

Fig. 3(a) shows magnetization (M) – field (H) curves of the $Co_{68}Pt_{32}$ sample deposited at −900 mV. The M-H curves revealed PMA in the $Co_{68}Pt_{32}$ layer. The other samples with compositions ranging from $Co_{44}Pt_{56}$ to $Co_{77}Pt_{23}$ also exhibited similar M-H curves, indicating PMA was robustly obtained in a

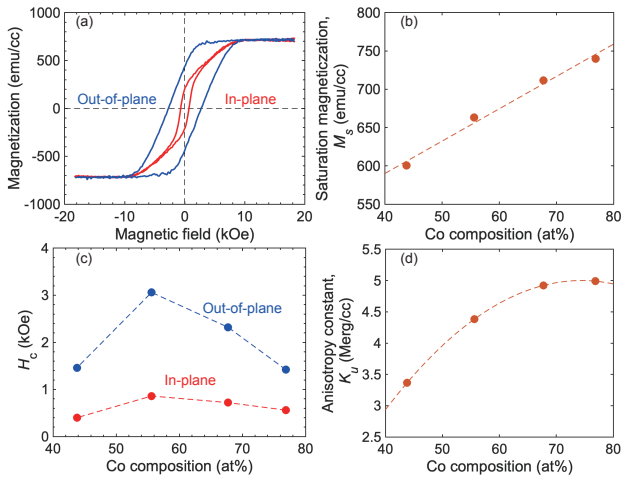

Fig. 3. (a) M-H curves of DC electrodeposited $Co_{68}Pt_{32}$ films formed at -900 mV. (b) M_s (c) H_c and (d) K_u dependence on the Co composition of CoPt films. The dotted curves are the guide for the eyes.

© 2023 IEEE. Personal use is permitted, but republication/redistribution requires IEEE permission. See https://www.ieee.org/publications/rights/index.html for more information.

This article has been accepted for publication in IEEE Transactions on Magnetics. This is the author's version which has not been fully edited and content may change prior to final publication. Citation information: DOI 10.1109/TMAG.2023.3298911

wide range of Co compositions in the CoPt films.

As shown in the red blues in Fig. 3(a) the in-plane *M-H* curves were slightly opened. This in-plane *M-H* curves can be decomposed into one curve with no H_c and one with H_c = 720 Oe, implying the easy axis was tilted or the two ferromagnetic phases coexisted. The saturation magnetic field for the out-of-plane curves was equal to the anisotropy magnetic field (H_k) in the in-plane *M-H* curves, implying granular-like magnetic behaviors.

Figs. 3(b), 3(c), and 3(d) exhibit saturation magnetization (M_s) and K_u, and H_c as a function of the Co composition. M_s increased with the increasing Co composition since the ferromagnetic element in the films increased. This dependence is consistent with the experimental results of CoPt thin films deposited using a sputtering technique [15]. Additionally, the maximum M_s value reached almost the same M_s used for a simulation of 3D-DWMM [2]. H_c depended on the Co composition as shown in Fig. 3(c). The out-of-plane curves exhibited larger H_c than the in-plane curves, supporting the PMA. K_u increased as the Co composition increased, then saturated at the Co composition of approximately 70%. These results manifest the successful control of magnetic properties.

Fig. 4(a) shows θ-2θ XRD patterns of the films with various compositions ranging from $Co_{44}Pt_{56}$ to $Co_{77}Pt_{23}$. CoPt in the hcp phase with *c*-axis orientation were obtained in all the films, regardless of Co composition. Since the *c*-axis corresponds to the easy axis of CoPt crystal in the hcp phase, we concluded that the PMA originated from the magnetocrystalline anisotropy. Note that the peaks at 2θ = 33.0° and 34.97° were Si (200) and Ti (100) diffraction, respectively [16,17].

Fig. 4 (b) shows lattice constant *c* extracted from the CoPt (002) and CoPt (004) diffraction peaks. *c* with respect to Co composition had a linear relationship, indicating the CoPt films

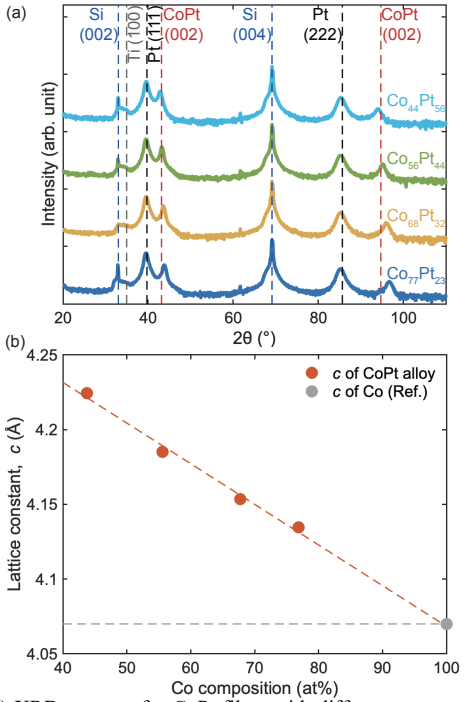

Fig. 4. (a) XRD patterns for CoPt films with different composition. (b) lattice constant *c* dependence on Co composition.

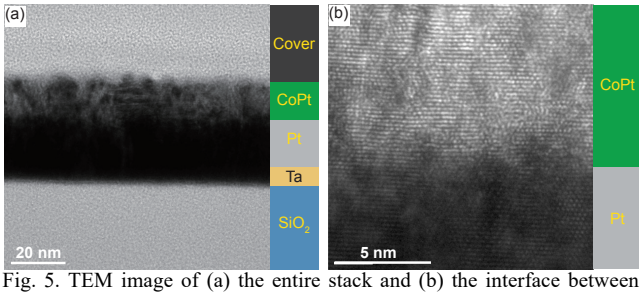

Fig. 5. TEM image of (a) the entire stack and (b) the interface between $Co_{68}Pt_{32}$ and Pt for a $Co_{68}Pt_{32}$ film formed at -900 mV.

followed the Vegard's law. The extrapolated *c* to the 100% of Co composition matches the literature data for pure Co [18], suggesting the presence of only a small number of impurities and strain in the films.

We conducted TEM observation for a 15 nm-thick $Co_{68}Pt_{32}$ film deposited at –900 mV to observe the microstructure and interface between the Pt and CoPt layers. Fig. 5(a) shows a bright field TEM image of the entire stack in a wide range view. A granular growth of CoPt grains was confirmed, consisting with the *M-H* curves. The peak-to-peak value of the surface was roughly calculated to be 5 nm. Fig. 5(b) shows a magnified view near the interface between the CoPt alloy and the Pt layers. The crystal lattice of hcp-CoPt was directly grown on the Pt (111) layer. The CoPt had a *c*-axis orientation which is consistent with XRD. The lattices were grown in the same orientation from the bottom to the top of CoPt. The interface between CoPt and Pt layer was smooth, which is promising for achieving the SOT-MS for the writing scheme of the 3D-DWMM [19,20].

B. Refinement of CoPt films by pulse electrodeposition

Next, we applied the pulse electrodeposition method to improve the surface morphology of CoPt films. During the off-time in the pulses, the growth of the grains can be suppressed, and atoms/ions are rearranged [21,22]. This process could result in even particle sizes and layer-by-layer growth.

Pulse electrodeposition experiments were carried out under the following conditions. The bath condition was the same as the DC method, as shown in Table I. The amplitude of a pulse current was set at 30 mA. The on-time and off-time were set at 10 ms and 5 ms, respectively. This pulse condition was chosen because the average potential under this pulse condition was -905 mV, which was close to the -900 mV applied in DC electrodeposition. Furthermore, the composition of the sample deposited by pulse electrodeposition was $Co_{68}Pt_{32}$, which is close to the sample deposited under -900 mV by DC electrodeposition as well.

Figs. 6(a) and 6(b) compare AFM images of $Co_{68}Pt_{32}$ ultra-thin films deposited with pulse and DC power, respectively.

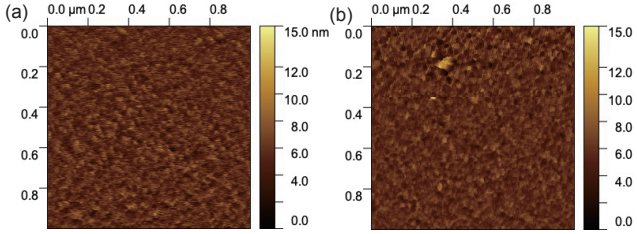

Fig. 6. AFM profiles of ultra-thin $Co_{68}Pt_{32}$ thin film deposited by (a) DC electrodeposition (b) pulse electrodeposition.

© 2023 IEEE. Personal use is permitted, but republication/redistribution requires IEEE permission. See https://www.ieee.org/publications/rights/index.html for more information.

This article has been accepted for publication in IEEE Transactions on Magnetics. This is the author's version which has not been fully edited and content may change prior to final publication. Citation information: DOI 10.1109/TMAG.2023.3298911

The thicknesses of the film were 7 nm and 10 nm, respectively. Average roughness (R_a) was 0.85 nm and 1.05 nm, respectively. A smooth surface was obtained for the pulse electrodeposition method, while holes-like defects were observed in the CoPt sample formed with the DC method.

The pulse electrodeposited $Co_{68}Pt_{32}$ film was further analyzed. Fig. 7(a) shows *M-H* curves of the 7 nm-thick CoPt film. The *M-H* curves exhibited strong PMA with a squareness ratio almost equal to one. H_s significantly decreased while H_k increased. M_s and K_u were 675 emu/cc and 5.5 Merg/cc, respectively. H_c along the out-of-plane direction was 1.9 kOe, which is slightly smaller than H_c of the $Co_{68}Pt_{32}$ film formed with the DC method. The opening of the in-plane *M-H* curve was less than that of the samples deposited by the DC method, indicating the pulse electrodeposited $Co_{68}Pt_{32}$ film showed more magnetically homogeneous. The reproducibility of $Co_{68}Pt_{32}$ ultra-thin film deposited by pulse electrodeposition was confirmed by over three times depositions and characterizations.

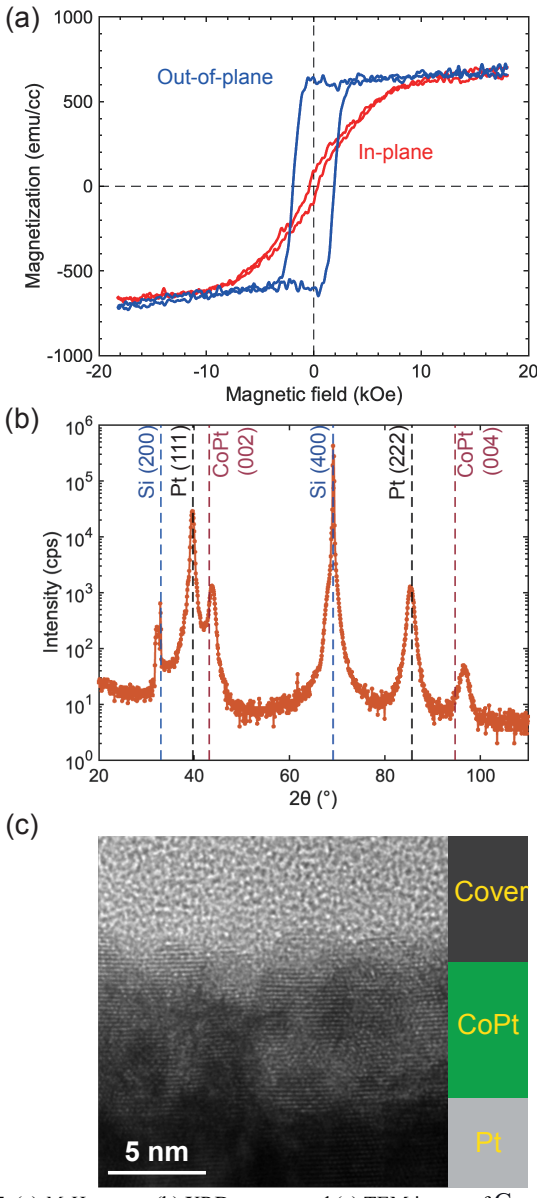

Fig. 7. (a) *M-H* curves, (b) XRD pattern and (c) TEM image of $Co_{68}Pt_{32}$ ultra-thin film deposited by pulse electrodeposition.

XRD analysis revealed that $Co_{68}Pt_{32}$ crystal in the hcp phase with (001) orientation was formed, as shown in Fig. 7(b). The XRD pattern also supports the PMA originating from the magnetocrystalline anisotropy. The lattice constant *c* was calculated to be 4.14 Å, the same as the DC electrodeposition sample with $Co_{68}Pt_{32}$ (c = 4.15 Å).

Fig. 7 (c) shows a TEM image of the pulse electrodeposited film. The TEM image revealed that the $Co_{68}Pt_{32}$ layer grew epitaxially and uniformly on the Pt underlayer. The $Co_{68}Pt_{32}$ crystal showed a single orientation, similar to the DC electrodeposition case. The peak-to-peak value was calculated as approximate 4 nm with this TEM image. A comparison of the TEM images (Figs. 5(a) and 7(c)) from the samples formed by the DC and pulse electrodeposition revealed no significant differences in surface roughness between the two samples. Considering the local insights provided by TEM and the more extensive area analysis based on the AFM images as shown in Fig. 6, we concluded the $Co_{68}Pt_{32}$ thin film deposited with pulse current exhibited an overall smoother surface.

IV. Conclusion

The electrodeposition techniques for CoPt thin films were established for three-dimensional domain motion memory (3D-DWMM). CoPt films with different compositions exhibited high controllability in magnetic properties and robust PMA. 7 nm thin $Co_{68}Pt_{32}$ alloy films were achieved by pulse electrodeposition. This ultra-thin $Co_{68}Pt_{32}$ film manifested strong PMA, good morphology, and epitaxial growth in hcp phase with *c*-axis orientation. These results could be applied to the multi-layered pillar of 3D-DWMM.

Acknowledgement

This work was supported by JST, CREST Grant Number JPMJCR21C1, Japan. The authors are grateful to Mr. Umebayashi, NIMS, Kyoto University Nanotechnology Hub, Electronic Material Characterization Shared Facility and Material Analysis Division, Open Facility Center, Tokyo Tech and Waseda University Nanotechnology Research Center for experimental support. The authors are also grateful to Prof. Ono, Kyoto University, Prof. Yamada, Gifu University and Prof. Homma, Waseda University for the fruitful discussions. The authors thank Mr. Y. Saito, Tokyo Institute of Technology for his support during experiments.

References

[1] Y.M. Hung, T. Li, R. Hisatomi, Y. Shiota, T. Moriyama and T. Ono, "Low Current Driven Vertical Domain Wall Motion Memory with an Artificial Ferromagnet," *J. Magn. Soc. Jpn.*, vol. 45, No. 1, pp. 6-11, Sept. 2020.

[2] Y.M. Hung, Y. Shiota, R. Hisatomi, T. Moriyama and T. Ono, "High thermal stability and low driven current achieved by vertical domain wall motion memory with artificial ferromagnet," *Appl. Phys. Express*, vol. 14, No. 2, pp. 023001.1-023001.4, Jan. 2021.

[3] A. Manchon, J. Železný, I.M. Miron, T, Jungwirth, J. Sinova, A. Thiaville, K. Garello and P. Gambardella, "Current-induced spin-orbit torques in ferromagnetic and antiferromagnetic systems," *Rev. of Mod. Phys.*, vol. 91, No. 3, pp. 035004-1-035004-80, Sept. 2019.

[4] Z. Wang, H. Cheng, K. Shi, Y. Liu, J. Qiao, D. Zhu, W. Cai, X. Zhang, S. Eimer, D. Zhu, J. Zhang, A. Fert and W. Zhao, "Modulation of field-like

© 2023 IEEE. Personal use is permitted, but republication/redistribution requires IEEE permission. See https://www.ieee.org/publications/rights/index.html for more information.

This article has been accepted for publication in IEEE Transactions on Magnetics. This is the author's version which has not been fully edited and content may change prior to final publication. Citation information: DOI 10.1109/TMAG.2023.3298911

spin orbit torque in heavy metal/ferromagnet heterostructures," *Nanoscale*, vol. 12, No. 28, pp. 15246-15251, Jun. 2020.

[5] L. Zhu, D.C. Ralph and R.A. Buhrman "Spin-orbit torques in heavy-metal–ferromagnet bilayers with varying strengths of interfacial spin-orbit coupling," *Phys. Rev. Lett.*, vol. 122, No.7, pp. 077201-1-077201-6, Feb. 2019.

[6] T. Shimatsu, H. Sato, T. Oikawa, Y. Inaba, O. Kitakami, S. Okamoto, H. Aoi, H. Muraoka and Y. Nakamura, "High-Potential Magnetic Anisotropy of CoPtCr-SiO_2 Perpendicular Recording Media," *IEEE Trans. Magn.*, vol. 41, No. 2, pp. 566-571, Feb. 2005.

[7] C. Eyrich, W. Huttema, M. Arora, et al. "Exchange stiffness in thin film Co alloys," J. Appl. Phys., vol. 111, No. 7, 07C919, Mar. 2012.

[8] I. Tabakovic, J.M. Qiu and O. Dragos, "Electrodeposition of thin CoPt films with very high perpendicular anisotropy from hexachloroplatinate solution: Effect of saccharin additive and electrode substrate," *J. Electrochem. Soc.*, vol. 163, No. 7, pp. D287-D294, Apr. 2016.

[9] S. Wodarz, T. Hasegawa, S. Ishio, and T. Homma, "Structural control of ultra-fine CoPt nanodot arrays via electrodeposition process," *J. Magn. Magn. Mater.*, vol. 430, No. 15, pp. 52–58, May 2017.

[10] Md. M. Hasan, T. Huang, M. saito, Y. Takamura, D. Oshima, T. Kato and T. Homma, "Electrodeposited CoPt multilayer nanowires for 3D memory device," *IEEE Xpress digital library*, to be published, 2023.

[11] Y. Miyazaki, T. Kajitani, "Preparation of Bi2Te3 films by electrodeposition," J. Cryst. Growth, No. 229, vol. 1-4, pp. 542-546., Jul. 2001.

[12] T. Homma, S. Wodarz, D. Nishiie, T. Otani, S. Ge and G. Zangari, "Fabrication of FePt and CoPt magnetic nanodot arrays by electrodeposition process," *ECS Trans.*, vol. 64, No. 31, pp. 1-9, Oct. 2014.

[13] A. Kahoul, F. Azizi, M. Bouaoud, "Effect of citrate additive on the electrodeposition and corrosion behaviour of Zn–Co alloy," *Int. J. Surf. Eng. Coat.*, vol. 95, No. 2, pp. 106-113, Mar. 2017.

[14] M.A.M. Ibrahim, R.M. Al Radadi, "Role of glycine as a complexing agent in nickel electrodeposition from acidic sulphate bath," *Int. J. Electrochem. Sci*., vol. 10, No. 6, pp. 4946-4971, Apr. 2015.

[15] N. Nozawa, S. Saito, S. Hinata and M. Takahashi, "Large uniaxial magnetocrystalline anisotropy for Co50Pt50 disordered alloy films with hexagonal-close-packed stacking structure by substituting Pt with Rh," *J. Phys. D: Appl. Phys.*, vol. 46, No. 17, 172001, 2013.

[16] P. Zaumseil, "High-resolution characterization of the forbidden Si 200 and Si 222 reflections," *J. Appl. Crystallogr.*, vol. 48, No. 2, pp. 528-532, 2015.

[17] A.V. Dobromyslov and N.I.Taluts, "Structure investigation of quenched and tempered alloys of the Zr-Ti system," *Phys. Met. Metallogr.*, vol. 63, pp. 114–120, 1987.

[18] T. Pan, G.W.D. Spratt, L. Tang and D.E. Langhlin, "Magnetic properties and microstructure of evaporated Co oxide tape media," *J. Magn. Magn. Mater.*, vol. 155, No. 1-3, pp. 309-311, Mar. 1996.

[19] M.A. Wahada, E. Şaşıoğlu, W. Hoppe, X. Zhou, H. Deniz, R. Rouzegar, T. Kampfrath, I. Mertig, S.S.P. Parkin and G. Woltersdorf, "Atomic scale control of spin current transmission at interfaces," *Nano Lett.*, vol. 22, No. 9, pp. 3539-3544, May 2022.

[20] N.H.D. Khang, Y. Ueda and N.H. Pham, "A conductive topological insulator with large spin Hall effect for ultralow power spin–orbit torque switching," *Nat. Mater.*, vol. 17, No. 9, pp. 808-813, Jul. 2018.

[21] S. Mandati, B.V. Sarada, S. R.Dey and S. V. Joshi, "Pulsed electrochemical deposition of $CuInSe_2$ and $Cu(In, Ga)Se_2$ semiconductor thin films," *Semiconductors–Growth and Characterization*, pp. 109-132, Dec. 2017.

[22] M. Paunovic and M. Schlesinger, *Fundamentals of electrochemical deposition*, pp. 307-318, Nov. 2005.

© 2023 IEEE. Personal use is permitted, but republication/redistribution requires IEEE permission. See https://www.ieee.org/publications/rights/index.html for more information.